

Chemical equilibration and thermal dilepton production from the quark gluon plasma at finite baryon density

D. Dutta, K. Kumar, A. K. Mohanty and R. K. Choudhury

Nuclear Physics Division, Bhabha Atomic Research Centre, Bombay-400085

(April 26, 2024)

Abstract

The chemical equilibration of a highly unsaturated quark-gluon plasma has been studied at finite baryon density. It is found that in the presence of small amount of baryon density, the chemical equilibration for gluon becomes slower and the temperature decreases less steeply as compared to the baryon free plasma. As a result, the space time integrated yield of dilepton is enhanced if the initial temperature of the plasma is held fixed. Even at a fixed initial energy density, the suppression of the dilepton yields at higher baryo-chemical potential is compensated, to a large extent, by the slow cooling of the plasma.

I. INTRODUCTION

One of the important objectives of all the future collider experiments at RHIC and LHC is to detect the new state of matter called quark gluon plasma (QGP) which is expected to be produced during the ultra-relativistic heavy ion collisions. Such an exotic state, if formed, will cool during expansion till it reaches a critical temperature T_c where the QGP will be transformed to the hadron phase via a first or second-order phase transition. The hadrons will then cool down further to the freeze-out temperature T_f where they cease to interact with each other and fly away to the detectors. During the process of the thermal expansion, photons and dileptons are produced directly from the plasma as well as from the hadron phases. These thermal photons and dileptons are considered to be ideal probes for the detection and study of subsequent evolution of the QGP [1] as they leave the plasma without any interaction.

In the standard scenario [2], the quark gluon plasma formed during the collision is expected to thermalize in a typical time scale of 1 fm/c. However, some recent works [3,4] suggest that due to high initial parton density (mostly gluonic) at RHIC and LHC energies, the

plasma may attain kinetic equilibrium in a very short time ($\tau \approx 0.3fm - 0.7fm$) but it may be far from chemical equilibrium. Since the initial parton plasma is mostly gluonic, many more quarks and anti-quarks are needed in order to achieve chemical equilibrium. Earlier studies [5–7] have shown that a chemically non-equilibrated plasma cools faster as compared to equilibrated plasma, which follows Bjorken’s scaling law ($T^3\tau = \text{const}$). In the case of non-equilibrated plasma, additional energy is consumed in producing more quarks and anti-quarks in approaching chemical equilibrium due to which the cooling is accelerated as compared to the Bjorken’s scaling law. Since the plasma cools faster, it may not attain chemical equilibrium before the temperature reaches the critical value T_c . Even if one includes transverse expansion, the large velocity gradient may drive the system further away from the chemical equilibrium as shown by [8].

The effect of chemical equilibration on thermal photon and dilepton emission has been studied by several authors [7–13]. In these studies, it was assumed that the nucleus-nucleus collision is fully transparent, leading to the formation of a baryon-free plasma. However, some of the recent works have suggested that even at RHIC energies the colliding nuclei may not be fully transparent and some amount of baryon stopping may occur particularly at higher rapidities. For $Au + Au$ collisions at 200 A GeV, the baryo-chemical potential μ_B may be of the order of T for $y \approx 2$ [14], which is the region of interest of the PHENIX detector for di-muon measurements [15]. The presence of finite baryon density may affect the process of chemical equilibration and the rate of cooling. This will, in turn, affect the thermal dilepton yields, which are the potential probes for the detection of the expanding quark gluon plasma.

The present work is aimed at studying these effects, by considering the dynamical evolution of a baryon rich plasma undergoing chemical equilibration. It is seen that the rate of cooling of the plasma slows down in the presence of μ_B compared to a baryon-free plasma. The calculations also show that the rate of dilepton production is suppressed at finite baryon density, but the time integrated thermal yields are rather unaffected due to slower cooling of the plasma in the presence of small amount of the baryon density.

II. CHEMICAL EQUILIBRATION

We assume a quark gluon plasma which has thermally equilibrated but is far off from chemical equilibrium. The distribution functions for quarks (anti-quarks) and gluons for such an unsaturated plasma can be described by Juttner distributions given by

$$f_q(\bar{q}) = \frac{\lambda_q(\bar{q})}{\lambda_q(\bar{q}) + e^{(p \mp \mu)/T}} = \frac{\lambda_q(\bar{q})e^{\pm x}}{\lambda_q(\bar{q})e^{\pm x} + e^{p/T}} \quad ; \quad f_g = \frac{\lambda_g}{e^{p/T} - \lambda_g} \quad (1)$$

where $x = \mu/T$. The fugacity factor λ_i ($i = q, \bar{q}$ and g) gives the measure of the deviation of the distribution functions from the equilibrium values and μ ($= \mu_B/3$) is the quark-chemical potential. The chemical equilibrium is said to be achieved when $\lambda_i \rightarrow 1$. It may be mentioned here that one can also define the quark and anti-quark distribution functions using a different definition for fugacities λ_Q and $\lambda_{\bar{Q}}$ given by

$$\lambda_Q(\bar{Q}) = e^{\pm x} \lambda_q(\bar{q}) \quad (2)$$

In that case, one does not use the quark chemical potential μ explicitly. However, the definition (1) is quite convenient, since at equilibrium ($\lambda_q = \lambda_{\bar{q}} = 1$), the chemical potential associated with λ_i vanishes but the baryo chemical potential still exists. Further, we have taken $\lambda_q = \lambda_{\bar{q}}$ at all values of τ so that when $\mu \rightarrow 0$, $\lambda_Q = \lambda_{\bar{Q}} = \lambda_q$ resulting in a baryon symmetric matter.

A. Rate equations

In general, chemical reactions among partons can be quite complicated because of the possibility of initial and final state gluon radiations. However, we restrict our considerations to the following dominant reaction mechanisms [5,7] for the equilibration of parton flavours,



The evolution of the parton densities are governed by the master equations

$$\partial_\mu(n_q u^\mu) = (R_{2 \rightarrow 3} - R_{3 \rightarrow 2}) - (R_{g \rightarrow q} - R_{q \rightarrow g}) \quad (3)$$

$$\partial_\mu(n_q u^\mu) = \partial_\mu(n_{\bar{q}} u^\mu) = (R_{g \rightarrow q} - R_{q \rightarrow g}) \quad (4)$$

where $R_{2 \rightarrow 3}$ and $R_{3 \rightarrow 2}$ denote the rates for the process $gg \rightarrow ggg$ and its reverse and $R_{g \rightarrow q}$ and $R_{q \rightarrow g}$ for the process $gg \rightarrow q\bar{q}$ and its reverse respectively. In case of a baryon rich plasma, the presence of quark-chemical potential μ , affects the process $gg \rightleftharpoons q\bar{q}$ directly. We, therefore, study the μ dependence of this process more explicitly. The rate equations for this process are given by [16]

$$R_{g \rightarrow q} = \frac{1}{2} \int \frac{d^3 p_1}{(2\pi)^3 2E_1} \int \frac{d^3 p_2}{(2\pi)^3 2E_2} \int \frac{d^3 p_3}{(2\pi)^3 2E_3} \int \frac{d^3 p_4}{(2\pi)^3 2E_4} (2\pi)^4 \delta^4(p_1 + p_2 - p_3 - p_4) \times$$

$$\sum |M_{gg \rightarrow q\bar{q}}|^2 f_g(p_1) f_g(p_2) [1 - f_q(p_3)] [1 - f_{\bar{q}}(p_4)] \quad (5)$$

and

$$R_{q \rightarrow g} = \frac{1}{2} \int \frac{d^3 p_1}{(2\pi)^3 2E_1} \int \frac{d^3 p_2}{(2\pi)^3 2E_2} \int \frac{d^3 p_3}{(2\pi)^3 2E_3} \int \frac{d^3 p_4}{(2\pi)^3 2E_4} (2\pi)^4 \delta^4(p_1 + p_2 - p_3 - p_4) \times \\ \sum |M_{q\bar{q} \rightarrow gg}|^2 f_q(p_3) f_{\bar{q}}(p_4) [1 + f_g(p_1)] [1 + f_g(p_2)] \quad (6)$$

In (5), the squared matrix element, summed over spin and color, $\sum |M|^2$ is weighted by two gluon distribution functions f_g for the initial states. The factor $[1 - f_q][1 - f_{\bar{q}}]$ indicates Pauli blocking for the final states. In the reverse process (6), the rate is weighted by the distribution functions of quarks and anti-quarks for the initial states and the gluon final states each gain an enhancement factor $[1 + f_g]$ due to Bose-Einstein statistics. The factor of 1/2 accounts for the identity of the two gluons.

Using the identity

$$[1 - f_q][1 - f_{\bar{q}}] = \frac{f_q(p_3) f_{\bar{q}}(p_4)}{\lambda_q \lambda_{\bar{q}}} e^{(p_3 + p_4)/T} \quad (7)$$

and

$$[1 + f_g(p_1)][1 + f_g(p_2)] = \frac{f_g(p_1) f_g(p_2)}{\lambda_g^2} e^{(p_1 + p_2)/T} \quad (8)$$

it may be shown that the μ dependence in the rate equations (5) and (6) for the process $gg \rightleftharpoons q\bar{q}$ basically comes through the product of quark and anti-quark distribution functions $f_q f_{\bar{q}}$.

Fig. 1(a) and (b) show the variation of the product $f_q f_{\bar{q}}$ with momenta p and λ_q respectively for different values of x . Fig. 1(a) shows the product $f_q f_{\bar{q}}$ as a function of p at a few typical values of x ($= \mu/T$) for $\lambda_q = 0.1$ and for temperatures $T=0.57$ GeV and $T=0.2$ GeV. Fig. 1(b) shows the $f_q f_{\bar{q}}$ as a function of λ_q at temperature $T=0.57$ GeV and $p=0$. It is seen (Fig 1a) that as the momentum increases or the temperature decreases, the $e^{p/T}$ factor in the denominator of (1) dominates and the product $f_q f_{\bar{q}}$ becomes less sensitive to μ . Here, we have used the same values of p for both quark and anti-quark distribution functions, although their momenta p_q and $p_{\bar{q}}$ can be quite different. However, for any other combinations of p_q and $p_{\bar{q}}$, the deviation will not be more than that observed for $p=0$. We have taken $p_q = p_{\bar{q}} = 0$ in Fig. 1(b) to show the maximum amount of deviation of this product as a function of λ_q . It can be seen from Fig 1(b), that the above product is not very sensitive to quark chemical potential if the plasma is highly unsaturated ($\lambda_q \leq 0.1$). This feature has an important relevance for the collisions at RHIC energy as the chemical equilibration is

not achieved by the time T drops to T_c and the quark fugacity remains much below unity ($\lambda_q \approx 0.1$) [5]. The nearly x independence of the above product is also evident from eq. (1). For small values of λ_q , the contribution from the factor $\lambda_q e^{\pm x}$ in the denominator is not very significant if x is small. The x dependence of the quark and anti-quark distribution functions mainly arises due to the $e^{\pm x}$ factor in the numerator. Since these exponential factors get cancelled in the product, $f_q f_{\bar{q}}$ will have weak x dependence at small baryon density if the plasma is highly unsaturated. So the integrals (5) and (6) will not depend explicitly on μ except through the thermal quark mass m_q^2 which is generally used as a cut-off parameter in the evaluation of the integral to avoid the divergence. The thermal quark mass appropriate for a non-equilibrium plasma is given by [17,18]

$$m_q^2 = \frac{g^2}{3\pi^2} \int_0^\infty dp p [2 f_g + f_q + f_{\bar{q}}] \quad (9)$$

Since the gluon distribution function has no μ dependence, the rate for the process $gg \rightleftharpoons ggg$ will depend on μ through the Debye screening mass m_D^2 which is used to avoid the divergence in both the scattering cross sections and the radiation amplitude and can be given by [19]

$$m_D^2 = \frac{3 g^2}{\pi^2} \int_0^\infty dp p [2 f_g + N_f (f_q + f_{\bar{q}})] \quad (10)$$

In the above, $N_f=2.5$ is the dynamical quark flavour and $g^2 = 4\pi\alpha_s$ is the strong coupling constants. The above rate equations have been solved by using the distribution function as discussed below.

B. Distribution function

In order to evaluate energy, number densities, thermal quark mass and Debye screening mass we consider the approximations for the quark and anti-quark distribution functions given by

$$f_{q(\bar{q})} = \frac{\lambda_{q(\bar{q})} e^{\pm \frac{\mu}{T}}}{\lambda_{q(\bar{q})} e^{\pm \mu/T} + e^{p/T}} \approx \frac{\lambda_{q(\bar{q})} e^{\pm x}}{1 + e^{p/T}} = \lambda_{q(\bar{q})} e^{\pm x} f_{q(\bar{q})}^{eq} \quad (11)$$

and gluon distribution function as

$$f_g = \lambda_g f_g^{eq} \quad (12)$$

where $f_{q(\bar{q})}^{eq} = (1 + e^{p/T})^{-1}$ and $f_g^{eq} = (e^{p/T} - 1)^{-1}$. For subsequent reference, we will call it as Modified Fermi Dirac type (MFD) approximation. It should be mentioned here that the most commonly used approximation (extended to non-zero μ) is given by

$$f_{q(\bar{q})} = \frac{\lambda_{q(\bar{q})}}{1 + e^{(p \mp \mu)/T}} \quad (13)$$

The above approximation becomes Fermi Dirac distribution in the limit $\lambda_q \rightarrow 1$ and we will refer it as FD type approximation. It has been shown in appendix A that this FD approximation is not strictly applicable in case of an unsaturated plasma (i.e. for $\lambda_i < 1$), though it has been used in all the earlier works [5–8,13] for baryon free plasma (i.e. $\mu = 0$). The MFD approximation (11) becomes FD type when $\mu \rightarrow 0$. We would also like to compare the MFD approximation with the Boltzmann (BM) approximation given by

$$f_q(\bar{q}) = \lambda_q(\bar{q})e^{-(p \mp \mu)/T} \quad (14)$$

The BM approximation is found to be closer to the anti-quark distribution function at finite baryon density. Comparison between different approximations has been discussed in appendix A.

We have evaluated the thermal quark mass m_q^2 numerically using (9) for various approximations as well as for the Juttner distribution. Fig. 2 shows m_q^2/T^2 as a function of λ_q at two different values of x . Here, the gluon contribution to thermal mass has not been included since we are interested only in examining the difference arising from the use of different approximation for the quark distribution function. It may be seen that the FD approximation coincides with the Juttner distribution only in the limit $\lambda_q \rightarrow 1$. However, in the region of interest i.e. λ_q up to 0.1 or 0.2, the deviation is quite significant. Similarly, the Boltzmann approximation agrees with the Juttner distribution only at very small values of λ_q while MFD approximation agrees with the Juttner distribution up to $\lambda_q \approx 0.35$ even at $x = 1.5$. Since the plasma is highly unsaturated to begin with and the quark fugacity remains much below unity, we will use the MFD approximation in the subsequent calculations. The advantage of using this approximation is that we can retain the factorisation used in [5] for the RHS of the rate equations (3) and (4) with the replacement of $\lambda_{q(\bar{q})}$ with $\lambda_{Q(\bar{Q})}$ (see appendix B for detail). The rate equations are then solved in the following way.

C. Formalism

We assume the system to undergo a purely boost invariant expansion. Using the MFD approximation, (3) and (4) can be written as

$$\partial_\mu(n_g u^\mu) = \frac{\partial n_g}{\partial \tau} + \frac{n_g}{\tau} = n_g R_3(1 - \lambda_g) - 2n_g R_2 \left(1 - \frac{\lambda_Q \lambda_{\bar{Q}}}{\lambda_g^2}\right) \quad (15)$$

$$\partial_\mu(n_q u^\mu) = \frac{\partial n_q}{\partial \tau} + \frac{n_q}{\tau} = n_g R_2 \left(1 - \frac{\lambda_Q \lambda_{\bar{Q}}}{\lambda_g^2}\right) \quad (16)$$

where $R_2 = \frac{1}{2}\sigma_2 n_g$ and $R_3 = \frac{1}{2}\sigma_3 n_g$ are the density weighted cross sections for the process $gg \rightleftharpoons qq$ and $gg \rightleftharpoons ggg$ respectively. Similarly, the equation for the conservation of energy and momentum can be written as

$$\frac{\partial \epsilon}{\partial \tau} + \frac{\epsilon + p}{\tau} = 0 \quad (17)$$

where the viscosity effect has been neglected [20]. In case of an ideal fluid, $3p = \epsilon$.

Using MFD approximation for quark, anti-quark (11) and gluon distribution functions (12), the energy density can be written as:

$$\epsilon = T^4 [a_2 \lambda_g + b_2 (\lambda_q e^x + \lambda_{\bar{q}} e^{-x})] \quad (18)$$

with $a_2 = 8\pi^2/15$; $b_2 = N_f(7\pi^2/40)$; where $N_f=2.5$ is the dynamical quark flavours. Similarly, the number densities for gluon, quark and anti-quark are:

$$n_g = \lambda_g a_1 T^3; \quad a_1 = \frac{16}{\pi^2} \zeta(3) \quad (19)$$

$$n_q = \lambda_q b_1 T^3 e^x; \quad b_1 = \frac{9}{2\pi^2} \zeta(3) N_f \quad (20)$$

$$n_{\bar{q}} = \lambda_{\bar{q}} b_1 T^3 e^{-x} \quad (21)$$

From the conservation of baryon number, one gets $\partial_\mu(n_B u^\mu) = 0$ which results in

$$n_B \tau = (n_q - n_{\bar{q}}) \tau = \text{const} \quad (22)$$

Using the expressions for the number and energy densities, the eq. (15,16) and (17,22) can now be written as

$$\frac{\dot{\lambda}_g}{\lambda_g} + \frac{3\dot{T}}{T} + \frac{1}{\tau} = R_3(1 - \lambda_g) - 2R_2 \left(1 - \frac{\lambda_Q \lambda_{\bar{Q}}}{\lambda_g^2}\right) \quad (23)$$

$$\frac{\dot{\lambda}_Q}{\lambda_Q} + \frac{3\dot{T}}{T} + \frac{1}{\tau} = R_2 \frac{a_1}{b_1} \frac{\lambda_g}{\lambda_Q} \left(1 - \frac{\lambda_Q \lambda_{\bar{Q}}}{\lambda_g^2}\right) \quad (24)$$

$$\dot{\lambda}_{\bar{Q}} = \dot{\lambda}_Q + \frac{\lambda_Q - \lambda_{\bar{Q}}}{\tau} + \frac{3\dot{T}}{T} (\lambda_Q - \lambda_{\bar{Q}}) \quad (25)$$

$$\frac{3\dot{T}}{T} + \frac{1}{\tau} = - \frac{3}{4 A_t} [a_2 \dot{\lambda}_g + b_2 \dot{\lambda}_Q + b_2 \dot{\lambda}_{\bar{Q}}] \quad (26)$$

where

$$A_t = a_2 \lambda_g + b_2 (\lambda_Q + \lambda_{\bar{Q}})$$

The above equations are solved numerically estimating R_2 and R_3 in a similar way as that of ref. [5,7]. Following ref. [5], the rate R_2 is written as

$$R_2 \approx .24 N_f \alpha_s^2 \lambda_g T \ln\left(\frac{1.65}{\alpha_s \lambda}\right) \quad (27)$$

where $\alpha_s (= 0.3)$ is the strong coupling constant. The factor $\lambda = (\lambda_g + \cosh x \lambda_q / 2)$ arises due to the thermal quark mass m_q^2 given by

$$m_q^2 = \frac{4\pi\alpha_s T^2}{9} [\lambda_g + \lambda_q \cosh x / 2] \quad (28)$$

which has been evaluated using MFD distribution functions. Following ref. [7], we estimate R_3 numerically

$$R_3/T = \frac{32}{3a_1} \frac{\alpha_s}{\lambda_g} \left[\lambda_g + \lambda_q \frac{N_f}{6} \cosh x \right]^2 \left[1 + \frac{2 m_D^2}{9 T^2} \right]^2 I(\lambda_g, \lambda_q, x) \quad (29)$$

where $I(\lambda_g, \lambda_q, x)$ is a function of λ_g, λ_q and x ,

$$I(\lambda_g, \lambda_q, x) = \int_1^{\sqrt{s}\lambda_f} dx \int_0^{s/4m_D^2} dz \frac{z}{(1+z)^2} \left[\frac{\cosh^{-1}(\sqrt{x})}{x\sqrt{[x + (1+z)x_D]^2 - 4xzx_D}} + \frac{1}{s\lambda_f^2} \frac{\cosh^{-1}(\sqrt{x})}{\sqrt{[1 + x(1+z)y_D]^2 - 4xzy_D}} \right] \quad (30)$$

with $x_D = m_D^2 \lambda_f$ and $y_D = m_D^2 / s$, $s = 18 T^2$ is the square of the average center of mass energy. The mean free path for elastic scattering is given by λ_f

$$\lambda_f^{-1} = \frac{9}{8} \alpha_s a_1 T \lambda_g \left[\lambda_g + \lambda_q \frac{N_f}{6} \cosh x \right]^{-1} \left[1 + \frac{2 m_D^2}{9 T^2} \right]^{-1} \quad (31)$$

The above equations (29-31) are similar as that of used in ref. [7] except it has been rederived to have x dependence through the Debye screening mass m_D^2 given by

$$m_D^2 = 4\pi\alpha_s T^2 \left[\lambda_g + \lambda_q \frac{N_f}{6} \cosh x \right] \quad (32)$$

derived using MFD distribution functions. It may be noted here that even in case of a baryon free plasma ($x=0$), the expression for m_D^2 still differs from $4\pi\alpha_s T^2 \lambda_g$ which has been used in ref. [5,7]. The rates R_2 and R_3 were calculated using the above equations. Fig. 3 shows

some typical results of the calculations of R_2/T and R_3/T as a function of λ_g for $x=0.0, 1.0$ and 1.5 . The values of $\lambda_q = \lambda_{\bar{q}}$ were fixed at $\lambda_g/5$. As can be seen, the equilibration rate R_3 initially increases and later on decreases with increasing baryon density whereas the rate R_2 is not affected much except at higher fugacities. This can be understood from the eq. (27) where R_2 has a logarithmic x dependence whereas R_3 depends on x more directly through the Debye screening mass m_D^2 (eq. 32). Also shown in the same figure are the results for R_3/T used in ref. [7] for $x=0$ (dot-dashed curve) with $m_D^2 = 4\pi\alpha_s T^2 \lambda_g$ which does not include the quark and anti-quark contributions. It is seen that, with the inclusion of quark and anti-quark contribution in the Debye screening mass, the rates R_3/T are lowered for $\lambda_g > 0.2$, but are enhanced for smaller λ_g values.

D. Results

The time dependence of $\lambda_g, \lambda_Q, \lambda_{\bar{Q}}$ and T were obtained by solving the set of rate eqs (23-26) numerically by fourth order Runge-Kutta method. We take the initial conditions from the Hijing calculations, $T_0 = 0.57$ GeV, $\lambda_{g0} = 0.09, \lambda_{q0} = 0.02$ at $\tau_0 = 0.31$ fm as used in [5] and treat x_0 as a parameter. We have carried out a parametric study to see the effect of chemical potential x on the chemical equilibration.

Figs. 4(a-d) show the temperature T , chemical potential $x = \mu/T$ and the fugacities ($\lambda_g, \lambda_q = \lambda_{\bar{q}}$) as a function of τ at few typical values of x_0 . Whether the plasma is baryon free or baryon rich, a common feature is that the process of chemical equilibration needs additional amount of energy which makes the plasma cool more rapidly than predicted by Bjorken's scaling $T^3\tau = \text{const}$ (dotted line, Fig. 4a). However, the plasma cools less rapidly in the presence of chemical potential compared to the baryon free plasma. Further, it is seen that the fugacity factors for gluon, quark and anti-quark do not reach the equilibrium values by the time the temperature T drops to the critical value $T_c \approx 0.2$ GeV (Fig. 4(c) and (d)). It is important to note that the gluon equilibration rate slows down in the presence of finite baryon density. On the other hand, the quark and anti-quark equilibration rates increase slightly in the presence of finite baryon density. As shown in Fig. 4(b), the chemical potential $x = \mu/T$ also decreases with τ . The overall effect, however, is that the plasma cools less rapidly in the presence of chemical potential as compared to the baryon free plasma.

The different behaviour of λ_g and λ_q observed in Figs 4(c) and 4(d) as a function of τ may be understood in the following way. The x dependence in the chemical equilibration arises due to the factors R_2, R_3 and baryon density (n_B) present in the rate equations (eq. 15 and eq. 16). As shown in Fig. 3, the rates R_2 and R_3 do not depend on x significantly. It was

found that even if R_2 and R_3 are made independent of x , i.e. if we drop the term containing $\lambda_q \cosh x$ in m_q^2 and m_D^2 completely, the rate of chemical equilibration is not affected much. Therefore, the slowing down of the gluon equilibration rate is not due to R_2 and R_3 , but due to the dynamical evolution of the plasma which is affected in the presence of baryon density (See Appendix C for detailed discussion). The finite baryon density makes the cooling rate slower as the plasma evolves with an additional constraint of baryon number conservation. This also effects the plasma density which is mostly gluonic. It may be mentioned here that even though R_2 and R_3 do not depend strongly on x , the rate of chemical equilibration ultimately depends on how fast the net parton production approaches zero, i.e. how fast the RHS of eq. (15) or eq. (16) becomes zero. Since initially $\lambda_g > \lambda_q$ and $R_3 > R_2$, a slight increase in gluon density produces more ggg as compared to $q\bar{q}$ or gg pairs (i.e. more gain than loss in the gluon numbers as seen from eq. 15). As a result, the gluon equilibration rate decreases where as the quark or anti-quark equilibration rate practically remains unchanged until at a later time when it goes up slightly. The decrease in gluon equilibration rate will consume less energy and will make the plasma cool still slower. Therefore, the over all slowing down of the plasma cooling rate is due to both slower gluon equilibration as well as a slower expansion rate of the plasma that results in presence of baryon density.

We have also investigated the rate of cooling by increasing the baryon density further, although our approximation breaks down at high x values. We find that the cooling rate never exceeds the Bjorken's limit which is consistent with the fact that for an ideal plasma Bjorken's scaling is the upper limit even in case of a baryon rich plasma. This may be verified directly from the conditions $s\tau = \text{const}$ and $n_B\tau = \text{const}$ (s and n_B are entropy and baryon density respectively) without solving any rate equations. For an equilibrated plasma, x remains independent of τ and the temperature follows the rule $T^3\tau = \text{const}$.

It is known that the rate of parton equilibration is enhanced considerably due to various factors like higher order gluon multiplication [21,22], temperature dependent coupling constants [23] and viscosity. All these processes need to be included for a complete understanding of the chemical equilibration during the hydrodynamical evolution of the plasma. We do not include all the above effects due to various complexities involved in the calculations. For example, the perturbative calculations may not be valid if α_s is allowed to vary with τ which may have large value at the end of the evolution [23]. Similarly, to calculate the rate for $gg \rightarrow (m-2)g$; $m > 5$, one needs to understand the complete space time structure of the multi gluon processes [22]. Similarly, inclusion of dissipative effects complicates the problem further. Therefore, in order to isolate the effect of baryo-chemical potential on the chemical equilibration, we have considered in this work a non-viscous plasma which

expands isentropically. We do not include any higher order gluon multiplication processes and also we use a constant value for $\alpha_s=0.3$. The results on the dilepton production yields are discussed in the following section.

III. DILEPTON PRODUCTION

Thermal photons and dileptons are the ideal probes to test the hydrodynamical evolution of a plasma created in heavy ion collisions at ultra-relativistic energies. It was shown in ref. [14,17] that the thermal photon and dilepton rates are suppressed at finite baryon density when the rates are calculated at a fixed energy density. However, this suppression is primarily due to lower initial temperature that results at higher baryon density. We will show in the following that the presence of finite baryon density enhances the space-time integrated thermal yield of dileptons, in spite of the fact that the rate of production is suppressed [14]. We have considered here the dilepton production, however this study can be extended to the thermal photons as well.

The dileptons are produced predominantly via the reaction $q^+q^- \rightarrow l^+l^-$. We ignore the annihilation and the Compton like reactions in the present calculations since their contributions may not be important for invariant masses above 1 GeV. The dilepton production rate $dN/(d^4x d^4p) = dR/d^4p$ (i.e. the number of dileptons produced per space time volume and four dimensional momentum volume) is given by:

$$\frac{dR}{d^4p} = \int \frac{d^3p_1}{(2\pi)^3} \int \frac{d^3p_2}{(2\pi)^3} f_q(p_1) f_{\bar{q}}(p_2) v_{q\bar{q}} \sigma_{q\bar{q}}^{l^+l^-} \delta^4(p - p_1 - p_2) \quad (33)$$

where $v_{q\bar{q}}$ is the relative velocity between quark and anti-quark and $\sigma_{q\bar{q}}^{l^+l^-}$ is the total cross section for the reaction $q\bar{q} \rightarrow l^+l^-$

$$\sigma_{q\bar{q}}^{l^+l^-} = \frac{4}{3} \frac{\pi \alpha^2}{M^2} \quad (34)$$

$M = p^\mu p_\mu$ is the invariant mass of the dileptons. The above integral can be simplified to [10]

$$\frac{dR}{dM^2} = \frac{5}{24\pi^4} M^2 \sigma(M^2) \int_0^\infty dp_1 f_q(p_1) \int_{M^2/4p_1}^\infty dp_2 f_{\bar{q}}(p_2) \quad (35)$$

We evaluate the above integral numerically using the exact definition of quark and anti-quark distribution functions as given by (1). Fig. 5(a) shows the plot of dR/dM^2 as a function of dilepton invariant mass at fixed initial temperature $T=0.57$ GeV corresponding to an equilibrated ($\lambda_q = 1.0$) and a non-equilibrated ($\lambda_q=0.2$ and 0.02) plasma. As can

be seen, the rate of dilepton production is not sensitive to x when the plasma is highly unsaturated (the lower curve for $\lambda_q = 0.02$). However, in case of an equilibrated plasma, it starts deviating more and more for higher x values (upper curve for $\lambda_q=1.0$). Since the plasma is highly unsaturated at the beginning ($\lambda_q \approx .02$) and reaches up to $\lambda_q \approx .2$ as it equilibrates, the rate of dilepton production will be insensitive to the small values of baryo-chemical potential. It can be mentioned here that we have also estimated the thermal dilepton production rate using the approximation (11). We do not find much difference with the actual calculations particularly when the plasma is unsaturated. This further justifies the use of the MFD approximation both for quark and anti-quark distributions. Next we calculate the integral over the space and time using the expression:

$$\frac{dN}{dydM^2} = \pi R_A^2 \int_{\tau_0}^{\tau_c} d\tau \tau \frac{dR}{dM^2} \quad (36)$$

The rate dR/dM^2 is estimated numerically using the exact distribution functions. However, for the space time evolution of the plasma at finite baryon density (i.e. for $T(\tau)$ and $\lambda_q(\tau)$), we use the results of the previous section which is obtained using the MFD approximation. Fig. 5(b) shows the above integrated yields at a fixed initial temperature of $T_0 = 0.57$ GeV and initial fugacities $\lambda_{g0} = 0.09$, $\lambda_{q0} = \lambda_{\bar{q}0} = 0.02$ for different values of x_0 . Although, the rate of dilepton production do not depend on x strongly, the space time integrated yield increases with x_0 due to slower cooling of the plasma in the presence of baryon density . Since the energy density is directly related to the experimental observables, we have also calculated the dilepton yield at a fixed initial energy density of $\epsilon_0 = 9$ GeV/fm³. This energy density corresponds to an initial temperature of $T_0 = 0.57$ GeV at $\lambda_{g0}=0.09$ and $\lambda_{q0} = 0.02$ when $x_0 = 0$. The results are shown in Figs. 6(a) and 6(b) for both the cases of equilibrated and non-equilibrated plasma. As shown in the figures, if the plasma is chemically non-equilibrated, the suppression of the dilepton yield at higher baryo-chemical potential is not significant even at higher invariant masses in contrast to the case for a chemically equilibrated plasma.

IV. CONCLUSION

In the present work, we have studied the effect of finite baryon density on the chemical equilibration of a longitudinally expanding quark gluon plasma. It is found that the rate of chemical equilibration for gluon slows down in the presence of finite baryon density in comparison to a baryon-free plasma, irrespective of various assumptions about the equilibration mechanism . This results in a slower cooling of the plasma , which has an important

consequence resulting in higher dilepton yields even though the rate of production may be suppressed at finite baryon density due to lower initial temperature. We have studied the thermal dilepton yields from the chemically non-equilibrated expanding plasma with finite baryon density . For calculating the dilepton yields, we have considered only an ideal non-viscous fluid that undergoes isentropic expansion and we have neglected higher order gluon processes as well as temperature dependence of the coupling constant. It is found that the space-time integrated yields of dileptons are enhanced if the initial temperature is held fixed. More importantly, even for a fixed initial energy density, the suppression of the yield at higher baryo-chemical potential is compensated to a large extent by the slow cooling of the plasma.

ACKNOWLEDGEMENT

We are thankful to Dr. D. K. Srivastava for illuminating discussions on several aspects of the present study.

APPENDIX A

Figs. A.1 and A.2 show the quark distribution function for $p=0$ and $p=0.5$ GeV as a function of λ_q at $x=1.0$. Figs. A.3 and A.4 show the corresponding plots for the anti-quark distributions. In all the cases, the FD approximations deviate significantly from the true Juttner distribution except when $\lambda \rightarrow 1$. This deviation is more significant in case of the baryon free plasma although the FD approximation has been used widely in all earlier calculations. At $x=0$, the BM distribution (not shown in the figure), is found to be closer to the Juttner distribution at small fugacities, but it starts deviating even at small λ when baryon density increases. On the other hand, the MFD approximation is relatively closer to the actual distribution over a wide range of fugacities (A.1 and A.2). However, the anti-quark distribution function (A.3 and A.4) becomes closer to BM approximation as x increases. At any momentum, for an unsaturated plasma at finite baryon density, the quark distribution function can be best described by the MFD approximation whereas the BM approximation is more suitable for the anti-quark distribution function. However, we do not want to use the MFD for f_q and BM for $f_{\bar{q}}$ as they will result in baryon asymmetry when $x \rightarrow 0$. Moreover, at finite baryon density, it is the f_q distribution which dominates as the anti-quarks are strongly suppressed (A.4). Therefore, we use the MFD approximation both for f_q and $f_{\bar{q}}$ in order to evaluate m_q^2 , m_D^2 and quark and anti-quark energy and number

densities. We have also solved the rate equations using BM approximation both for quark and anti-quark distributions, but the final results do not change much. This is primarily due to the fact that the x dependence comes through the exponential $e^{\pm x}$ in the numerator of eq. (1) and it does not matter if one uses BM or MFD approximations. However, we have used the MFD approximation for the calculations so that the same parametrization of ref. [5] can be employed by solving the rate equations.

APPENDIX B

For a baryon free plasma ($\mu = 0$), Biro et. al. have used a simple factorisation for the rate equations. We can retain the same factorisation for both the processes $gg \rightleftharpoons q\bar{q}$ and $gg \rightleftharpoons ggg$ (eq.(3) and (4)) under the MFD approximations. Using the identity (7,8) and the MFD approximations (11,12) for quark, anti-quark and gluons, the gain and loss terms for the process $gg \rightleftharpoons ggg$ (eq. (5) and (6)) can be combined to give

$$R_{g \rightarrow g} - R_{q \rightarrow g} = (\lambda_g^2 - \lambda_Q \lambda_{\bar{Q}}) \frac{1}{2} \int \frac{d^3 p_1}{(2\pi)^3 2E_1} \int \frac{d^3 p_2}{(2\pi)^3 2E_2} \int \frac{d^3 p_3}{(2\pi)^3 2E_3} \int \frac{d^3 p_4}{(2\pi)^3 2E_4} \times \\ (2\pi)^4 \delta^4(p_1 + p_2 - p_3 - p_4) \sum |M|^2 f_q^{eq}(p_3) f_{\bar{q}}^{eq}(p_4) f_g^{eq}(p_1) f_g^{eq}(p_2) e^{\frac{E_1 + E_2}{T}} \quad (\text{B.1})$$

where $p_1 + p_2 = E_1 + E_2$ for mass less quarks or gluons. From the above expression, it is clear that the right hand side vanishes when $\lambda_g = \lambda_q = \lambda_{\bar{q}} = 1$. Since the plasma is highly unsaturated, it may be reasonable to replace f^{eq} with the Boltzmann distribution. The integral in eq. (B.1) can be written as

$$I = \frac{1}{2} \int \frac{d^3 p_1}{(2\pi)^3} \int \frac{d^3 p_2}{(2\pi)^3} [\sigma_{gg \rightarrow q\bar{q}} v_{12}] f_g(p_1) f_g(p_2) \quad (\text{B.2})$$

which represents the free space cross section for the process $gg \rightarrow q\bar{q}$ folded with the distributions for the initial particles. The cross section $\sigma_{gg \rightarrow q\bar{q}}$ is given by

$$\sigma_{gg \rightarrow q\bar{q}} = \frac{1}{v_{12} 2E_1 2E_2} \int \frac{d^3 p_3}{(2\pi)^3 2E_3} \int \frac{d^3 p_4}{(2\pi)^3 2E_4} (2\pi)^4 \delta^4(p_1 + p_2 - p_3 - p_4) \sum |M|^2 \quad (\text{B.3})$$

It can be mentioned here that the above integral (B.2) is identical to the one which could have been obtained with the classical approximations, i.e. using the Boltzmann distribution function for quark, anti-quark and gluon and eliminating the Pauli blocking and Bose enhancement factors in the final states in (5) and (6). Although, we use the quantum statistics, the same expression is obtained as the classical one due to the identity and the approximations eqs. (7,8,11,12). However Boltzmann approximation is used finally for f^{eq} .

Following [5], eq. (B.2) can be factorised as

$$R_{g \rightarrow g} - R_{q \rightarrow g} = \frac{1}{2} \sigma_2 n_g^2 \left(1 - \frac{\lambda_q \lambda_{\bar{q}}}{\lambda_g^2}\right) \quad (\text{B.4})$$

Similarly for the rate $gg \rightarrow ggg$, one can use

$$R_{2 \rightarrow 3} - R_{3 \rightarrow 2} = \frac{1}{2} \sigma_3 n_g^2 (1 - \lambda_g) \quad (\text{B.5})$$

where

$$\sigma_2 = \langle \sigma(gg \rightarrow q\bar{q})v \rangle, \quad \sigma_3 = \langle \sigma(gg \rightarrow q\bar{q})v \rangle$$

V. APPENDIX C

The quark gluon plasma in (1+1) dimension expands following the scaling law $T^3 \tau = \text{const}$. If, chemical equilibration is not complete, the plasma cools faster than $t^{-1/3}$ as additional energy is spent in chemical equilibration. Therefore, in case of a chemically equilibrating plasma, the cooling rate depends on the rate of equilibration of quarks and gluons present in the plasma. Further, as shown in the text, the presence of baryo-chemical potential makes the gluon equilibration slow and also the temperature of the plasma falls slowly in comparison to the baryon free case. However, as will be shown here, the slow cooling of the plasma is not entirely due to the decrease of the gluon equilibration rate, but also due to the presence of baryo-chemical potential which effects the hydrodynamical expansion of the plasma. This has been demonstrated in fig. C where the temperature T , the gluon (λ_g) and quark (λ_q) fugacities have been plotted as a function of τ both for baryon free and baryon rich cases ($x=0$ and 2.0 , see the solid and dashed curves). As discussed in the text, the gluon equilibration rate slows down and the plasma cools slowly when the baryon density is finite where as the quark equilibration rate is not effected much. Next, we consider only a baryon free plasma, but we try to reduce the gluon and the quark equilibration rate by reducing the rate R_3 and R_2 by a factor $f=0.6$ so that the plasma now cools with the same rate (see the dotted line) as that of baryon rich case with $x=2.0$ (dashed curve obtained using the normal value of R_2 and R_3). However, the equilibration rates for gluon and quarks now become much slower (dotted lines) as compared to the dashed curves. This indicates that if the plasma needs to cool with a rate as that of dashed curve just due to chemical equilibration alone, the gluon and quarks need to equilibrate with a rate much slower than what is shown in fig. C corresponding to the case of a baryon rich plasma. In other words, a higher equilibration rate of gluon and quark as that of dashed curves will consume more energy and the plasma will cool faster than what is shown by dashed curve (but still slower than the solid line) had the chemical equilibration been the only reason for

the deviation of the cooling of the plasma from the Bjorken's scaling. Therefore, in presence of baryon density, the slow cooling rate of the plasma arises due to two factors; one being the slow gluon equilibration rate which consumes less energy. The other one is due to the slow hydro-dynamical expansion as the plasma now needs to expand conserving the baryon number as well.

REFERENCES

- [1] J. Alam, S. Raha and B. Sinha, Phys. Rep. **273**, 243 (1996).
- [2] J. D. Bjorken, Phys. Rev. **D27**, 140 (1983)
- [3] E. Shuryak, Phys. Rev. Lett. **68**, 3270 (1992).
- [4] K. J. Eskola and X. N. Wang, Phys. Rev. **D49**, 1284 (1994).
- [5] T.S. Biro, E. van Doorn, B. Muller, M. H. Thoma and X. N. Wang, Phys. Rev. **C 34** 1275 (1993).
- [6] T. S. Biro, B. Muller, M. H. Thoma and X. N. Wang, Nucl. Phys. **A566**, 543c (1995).
- [7] P. Levai, B. Muller and X. N. Wang, Phys. Rev. **C51**, 3326 (1995).
- [8] D. K. Srivastava, M. G. Mustafa and B. Muller, Phys. Lett. **B396**, 451 (1997).
- [9] E. Shuryak and L. Xiong, Phys. Rev. Lett. **70**, 2241 (1993).
- [10] M. Strickland, Phys. Lett. **B331**, 245 (1994).
- [11] B. Kampfer, O. P. Pavlenko, A. Peshier and G. Soff, Phys. Rev. **C52**, 2704 (1995).
- [12] C. T. Traxler and M. H. Thoma, Phys. Rev. **C53**, 1348 (1996).
- [13] D. K. Srivastava, M. G. Mustafa and B. Muller, Phys. Rev. **C56**, 1064 (1997).
- [14] A. Dumitru, D. H. Rischke, T. Schonfeld, L. Winckelmann, H. Stocker and W. Greiner, Phys. Rev. Lett. **70**, 2860 (1993); A. Dumitru, D. H. Rischke, H. Stocker and W. Greiner, Mod. Phys. Lett. A8, 1291 (1993) and references therein.
- [15] PHENIX conceptual design report, 1995 (unpublished).
- [16] T. Matsui, B. Svetitsky and L. McLerran, Phys. Rev. **D34**, 783 (1986).
- [17] H. Vija and M. H. Thoma, Phys. Lett. **B346**, 329 (1995).
- [18] R. Baier, M. Dirks, K. Redlich and D. Schiff, Phys. Rev. **D56**, 2548 (1997)
- [19] T. S. Biro, B. Muller and X. N. Wang, Phys. Lett. **B283**, 171 (1992).
- [20] P. Danielewicz and M. Gyulassy, Phys. Rev. **D31**, 53 (1985).
- [21] L. Xiong and E. Shuryak, Phys. Rev. **C49**, 2203 (1994).
- [22] X. N. Wang, Phys. Rep. **280**, 291 (1997).

[23] S. M. H. Wong, Phys. Rev. **C54**, 2588 (1996); Phys. Rev. **C56** , 1075 (1997).

- Fig. 1

(a) The product of quark and anti-quark distribution function as a function of p for different values of x at $T = 0.57$ GeV and 0.2 GeV. (b) Same as (a), but as a function of λ_q .
- Fig. 2

The thermal quark mass m_q^2/T^2 versus λ_q at $x = 1.0$ and $x = 1.5$ (the upper curves are increased by one unit). The solid curve is for the Juttner distribution function (eq. 1). The other curves are obtained using different approximations, MFD (eq. 11), FD (eq. 13) and BM (eq. 14) respectively.
- Fig. 3

The gluon production rate, R_3/T , and quark production rate R_2/T as function of λ_g ($\lambda_q = \lambda_{\bar{q}} = \lambda_g/5$) for $x = 0.0, 1.0$ and 1.5 . The dashed dot curve is for R_3/T at $x = 0.0$ with $m_D^2 = 4\pi\alpha_s T^2 \lambda_g$ as used in ref. [7].
- Fig. 4

(a) The temperature, (b) the quark chemical potential $x = \mu/T$, (c) the gluon fugacity λ_g , (d) the quark fugacity λ_q , as a function of τ for $x_0 = 0.0, 1.0$ and 1.5 with the initial conditions $T_0 = 0.57$ GeV, $\lambda_{g0} = 0.09$ and $\lambda_{q0} = 0.02$. The dotted line in (a) corresponds to the temperature as per the Bjorken's scaling.
- Fig. 5

(a) The dilepton production rate dR/dM^2 as a function of invariant mass M for $\lambda_q = 0.02, 0.2$ and 1.0 . The initial temperature of the plasma is $T_0 = 0.57$ GeV. (b) The space time integrated dilepton yield versus invariant mass M for a chemically non-equilibrated plasma ($\lambda_{g0}=0.09, \lambda_{q0}=0.02$) at a fixed initial temperature of $T_0 = 0.57$ GeV with $x_0 = 0.0, 1.0$ and 1.5 .
- Fig. 6

(a) The integrated dilepton yield from a chemically equilibrated plasma at a fixed initial energy density for various values of x_0 . (b) Same as Fig. 6(a), but from a chemically non-equilibrated plasma.
- Fig. A

The quark (f_q) and anti-quark ($f_{\bar{q}}$) distribution functions versus λ_q at $p = 0$ (A.1 and A.3) and $p = 0.5$ GeV (A.2 and A.4).

FIGURES

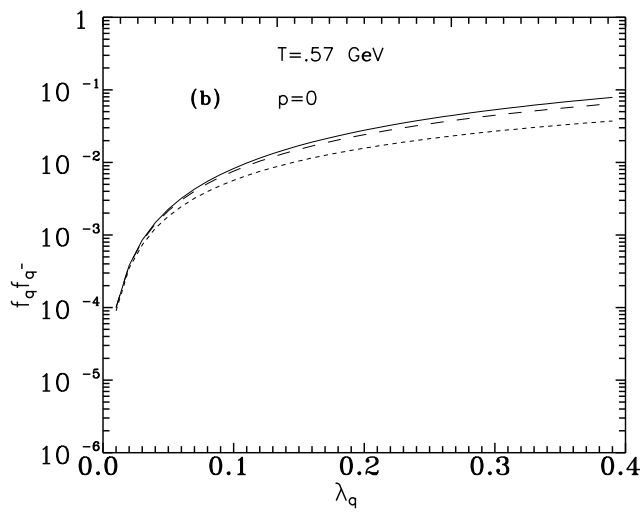
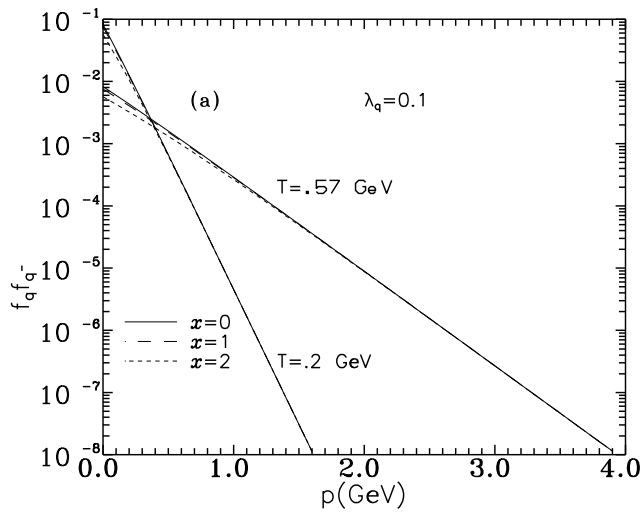


Fig. 1

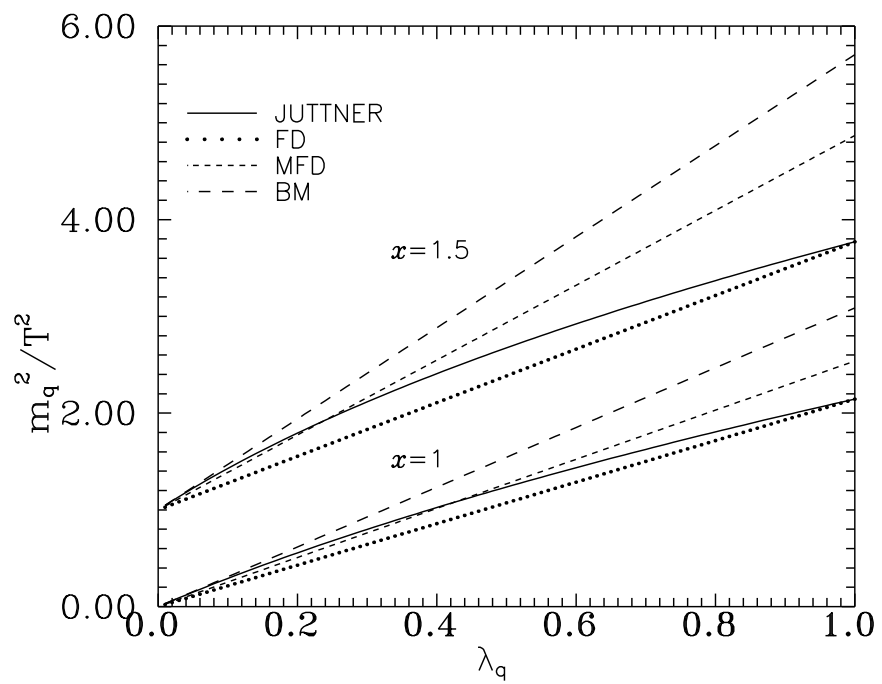


Fig. 2

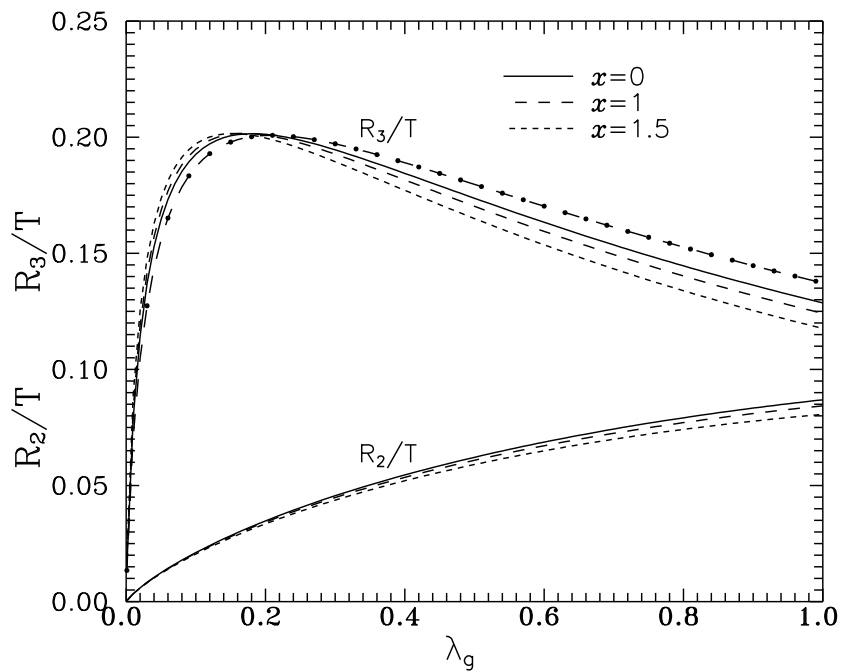


Fig. 3

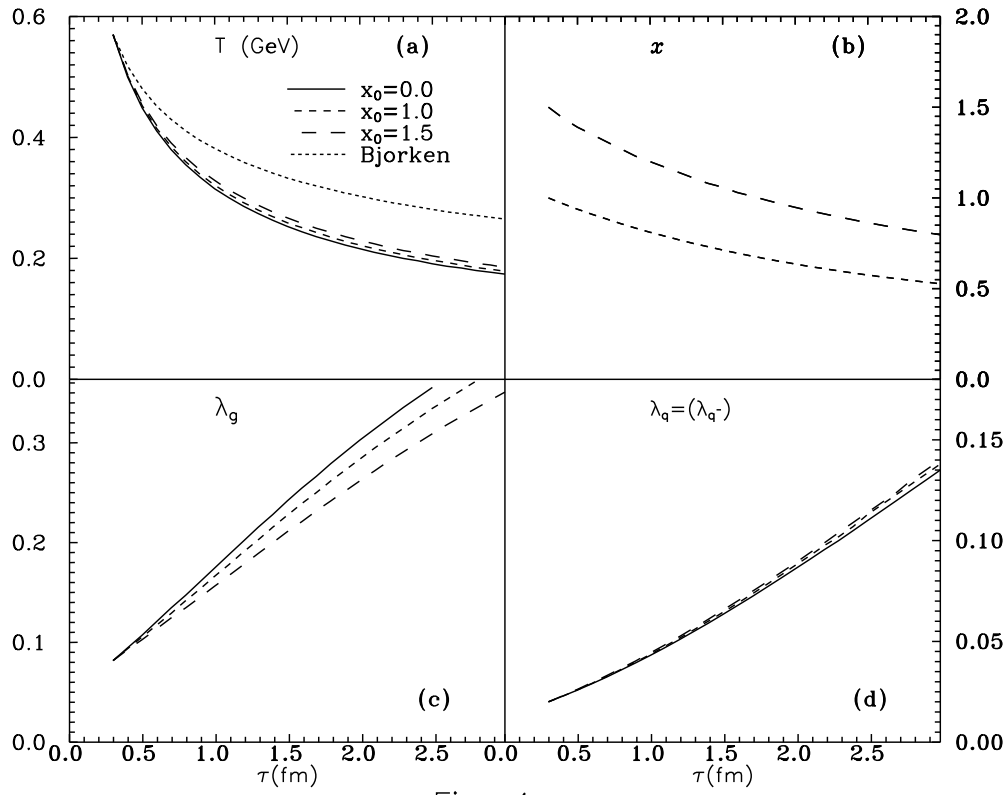


Fig. 4

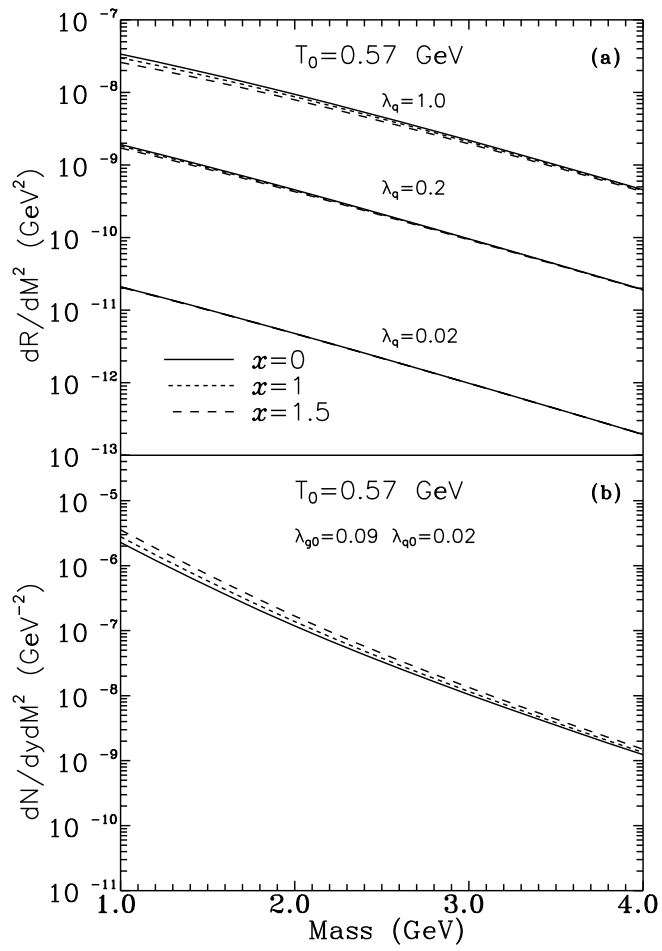


Fig. 5

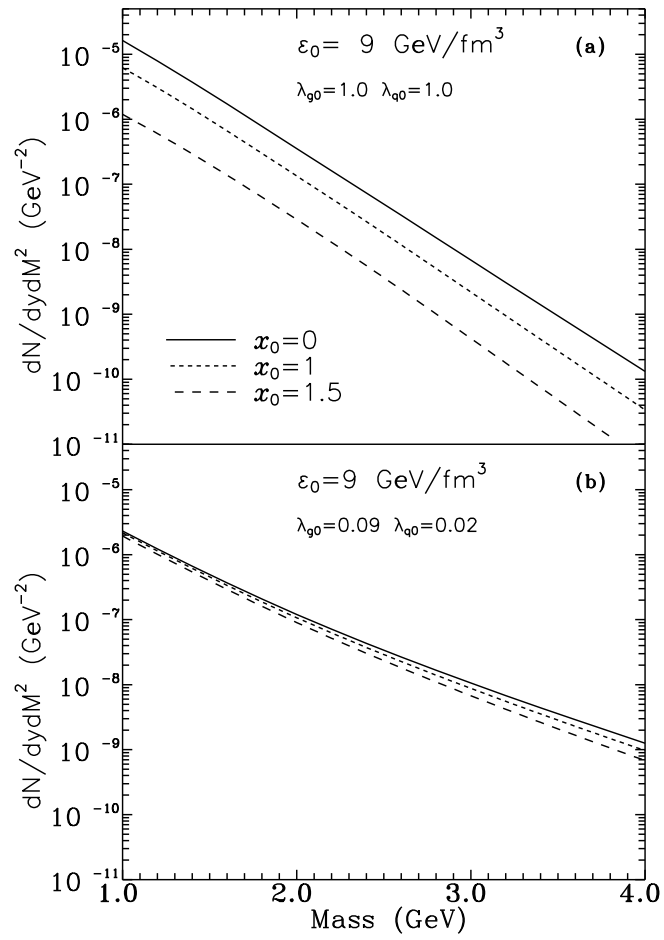
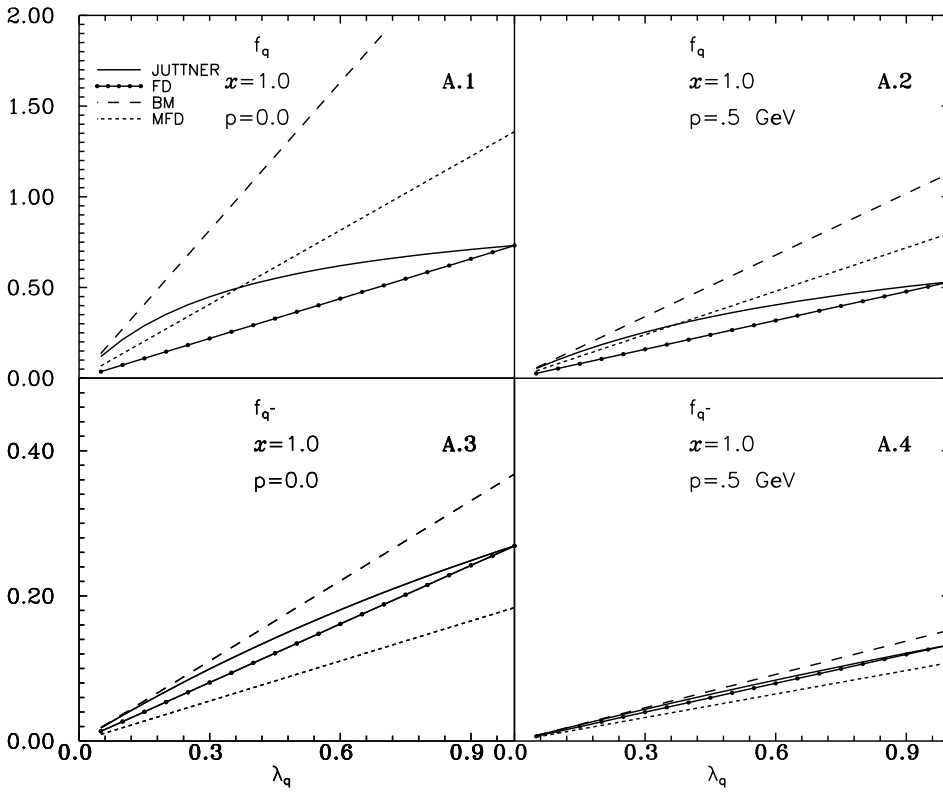


Fig. 6



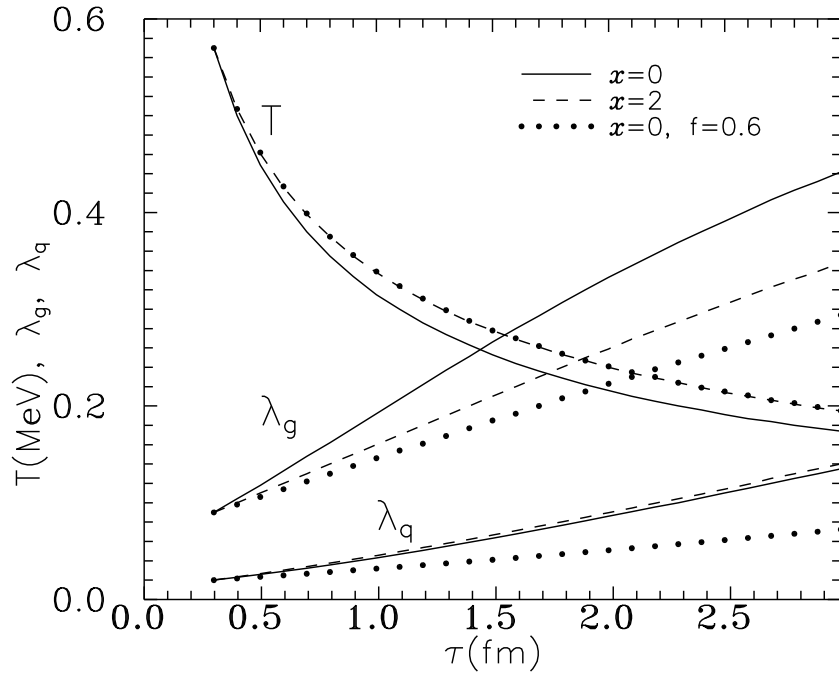


Fig. C